

Impact of the observed extratropics on climatological simulations of the MJO in a tropical channel model

Nicholas M. J. Hall¹ · Séverin Thibaut¹ · Patrick Marchesiello¹

Received: 17 December 2015 / Accepted: 3 June 2016 / Published online: 15 June 2016
© Springer-Verlag Berlin Heidelberg 2016

Abstract A regional model is used to quantify the influence of the extratropics on simulated tropical intraseasonal variability. The Weather Research and Forecasting (WRF) model is run in tropical channel mode with the boundaries at 30°N and S constrained to 6-hourly reanalysis data. Experiments with modified boundary conditions are carried out in which intraseasonal (20–100 days) timescales are removed, or in which only the annual and diurnal cycles are retained. Twin runs are used to give an objective measure of the boundary-independent component of the variance in each case. The model captures MJO-like propagating structures and shows greater zonal-wind variance in runs with full boundary conditions. Comparison between experiments indicates that about half the intraseasonal variance can be attributed to boundary influence, and specifically to the presence of an intraseasonal extratropical signal. This signal is associated with stronger correlations between low-level zonal wind precursors in the Pacific sector and Indian Ocean convective events. Temporal coherence between MJO events in the model and the observations is analysed by defining four phases based on convectively coupled signals in the low-level zonal wind. The model can only match observed events above the level of chance when intraseasonal boundary information is provided. Results are analysed in terms of ‘primary’ and ‘successive’ events. Although the model hindcast skill is generally poor, it is better for successive events.

Keywords MJO · Intraseasonal variability · Tropical-extratropical interactions · Regional model · WRF

1 Introduction

Tropical intraseasonal variability in the atmosphere is characterised by large-scale propagating signals that interact with convection, particularly in the eastern hemisphere (Salby and Hendon 1994). Their convective signature stands out from the background noise in space-time spectra (Wheeler and Kiladis 1999) and can be associated with Rossby and Kelvin wave modes and the Madden Julian Oscillation (MJO: Madden and Julian 1971, 1972; see Zhang 2005; Lau and Waliser 2012 for recent reviews). The relationship between the various propagating modes is a subject of perennial interest (Hendon and Salby 1994; Roundy 2008; Dias et al. 2013) and is clearly of great importance for understanding intraseasonal variability. The state of the MJO in particular has been shown to have implications for medium to long range forecasting both in the tropics (Flatau et al. 2001, 2003; Bellenger and Duvel 2007; Vitart and Jung 2010) and in the extratropics (Ferranti et al. 1990; Hendon et al. 2000; Jung et al. 2010).

Faithful simulation of the MJO remains a challenge for numerical models. Current GCMs are able to simulate the salient features with varying degrees of success (Hung et al. 2013) and multiple factors have been found to be important, including resolution, convection, simulation of mean winds, sea surface temperature (SST) distributions and atmosphere-ocean coupling, including wind-induced surface fluxes (see for example, Inness and Slingo 2003; Maloney and Sobel 2004; Woolnough et al. 2007; Landu and Maloney 2011; Crueger et al. 2013). Aside from the general problem of capturing MJO-like statistics,

LEGOS, University of Toulouse, UPS, IRD, CNRS, CNES.

✉ Nicholas M. J. Hall
Nick.Hall@legos.obs-mip.fr

¹ LEGOS, 14 Ave. Edouard Belin, 31400 Toulouse, France

models can also have difficulty propagating some cases from observed initial conditions (Ray and Zhang 2010). So there are multiple difficulties in simulating the MJO associated mainly with the representation of convection and its interaction with dynamics, and with the initiation of events. In this paper we will concentrate on the latter aspect, and show some quantitative results concerning the potential of boundary conditions to provide this initiation.

There is documented coherence between tropical and midlatitude propagating signals (Knutson and Weickmann 1987; Straus and Lindzen 2000; Zhou and Miller 2005; L'Heureux and Higgins 2008; Weickmann and Berry 2009). It is also possible that global modes can span the two systems (Frederiksen and Frederiksen 1997; Frederiksen 2002; Frederiksen and Lin 2013). Beyond simple coherence, evidence has also been found for causal extratropical influence on tropical intraseasonal variability. Yanai and Lu (1983) found meridional convergence of wave energy flux to be associated with equatorially trapped modes and Liebmann and Hartmann (1984) showed that extratropical geopotential predominantly leads intraseasonal tropical OLR.

Mechanisms put forward include the initiation of tropical convection by extratropical Rossby waves (Hsu et al. 1990; Matthews and Kiladis 1999). These studies emphasise the importance of the extratropical wave guide in determining the longitude of the extratropical influence. Rossby waves can penetrate the tropics in the central Pacific upper level westerlies, although Hoskins and Yang (2000) have shown that a moving vorticity source can excite tropical Kelvin waves at other longitudes. In simple modelling studies eastern hemisphere tropical Kelvin waves have also been excited by transient wave activity in the North Atlantic (Lin et al. 2007) and in the Eurasian sector (Pan and Li 2008). Intrusions from the southern hemisphere are also implicated: Kerns and Chen (2014) show an example for the November 2011 MJO event which took place during the DYNAMO field campaign (Yoneyama et al. 2013).

Matthews (2008 hereafter M08) has classified Madden-Julian events as 'primary' or 'successive' depending on whether they arise spontaneously or follow on directly from a previous event. He found that primary events tend to have their origins within the tropics but successive events can be initiated from outside the tropics. This suggests a complex chain of events in which the MJO can influence the extratropics and then in turn be influenced by the extratropics. Circulation anomalies associated with MJO convective heating can draw in heat and moisture fluxes from outside the tropics. The MJO can precondition the tropical atmosphere to respond to an incoming disturbance (Zhao et al. 2013) and extratropical waves emanating from MJO convection can be guided back into the tropics by the subtropical jets, and subsequently influence the MJO downstream (Moore et al. 2010; Roundy 2012). A recent

diagnostic study by Adames et al. (2014) could potentially clarify the tropical-extratropical separation by dividing the global circulation into tropical and extratropical sources of vorticity and divergence to identify extratropical wavetrains that are independent of MJO sources. But in all such studies, a definition is still required for the tropics.

Model simulations of the tropical band that impose observational (re)analyses on the boundaries can also encounter this separation problem. Wherever one decides to define the limit between tropics and extratropics, the values of atmospheric variables on this boundary may be influenced by observed variability both from the tropics and the extratropics. So if this information is used as a boundary condition, and subsequently imposed on a tropics-only run, there is a risk of reintroducing temporal information that originated from the tropics back into the tropics. The farther the zonal boundaries are placed from the equator, the less severe this problem will be, but then the desired extratropical influence will also be reduced.

In a set of eastern-hemisphere regional model runs intended to isolate the influence of the extratropics, Gustafson and Weare (2004a, b) imposed 6-hourly reanalyses at 24°N and S. When they removed the 30–70 day period in the boundary conditions it had little influence on the mean flow but weakened their MJO signal, without, however, completely eliminating it. Ray et al. (2009) and Ray and Zhang (2010) extended this type of study to the entire tropical channel between 21°N and S. They found that the presence of a correctly phased time-varying signal on the boundaries was critical to the successful initiation of the MJO in two case studies. Their conclusions held for boundaries as far as 38° from the equator. Ray et al. (2011) then identified an event that was not captured by their model, even with the correct boundary conditions, implicating the importance of a correct model mean state. Similar experiments have been performed by Vitart and Jung (2010) using extratropical relaxation in a series of hindcasts with a global forecasting system. They found that the central North Pacific region, where Rossby waves can penetrate into the tropics, is particularly important for skilful MJO forecasts.

The influence of boundary transients on tropical channel simulations is also likely to affect the model's representation of the MJO indirectly, since synoptic scale momentum fluxes help maintain the tropical mean state. Studies using full GCMs have underlined this point. Ray and Li (2013) found that removing transients poleward of 20°N and S had more effect on their MJO simulation than did blocking the zonal propagation, mainly because of the detrimental effect on the model climatology. In a recent simple GCM study Ding and Kuang (2016) claim that this is indeed the predominant influence from the extratropics, and they remedy this problem by restoring the tropical mean state.

It is useful to be able to compare model simulations with observed MJO test cases. The use of reanalysis data for boundary conditions allows this connection with real time series in long integrations. It is also desirable to run simulations for long enough to permit more general and systematic inferences to be drawn on the nature of the intraseasonal variability and its connection with the extratropics. In this study we present a set of climatological (20-year) integrations of a regional atmospheric model over the entire tropical band. To our knowledge this is the first time such experiments have been carried out using observed boundary conditions over such long integrations. We also present some experiments designed to isolate the internal part of the tropical variability that is formally independent of the boundary conditions. This is achieved by examining the difference between twin integrations which use identical boundary conditions. The integrations differ only in their initial conditions. The difference between them can be viewed as internal tropical variability, which is nonetheless consistent with the presence of realistic time-varying boundary conditions. Since the twin experiments have almost identical time-mean states, quantities related to the variance of each single integration, and to the variance of the difference between them, can be examined on an equal footing. We also use this experimental setup with time-filtered lateral boundary conditions and SSTs in a similar manner to Gustafson and Weare (2004b) to assess the impact of synoptic and intraseasonal timescales in the extratropics. Mixed boundary condition experiments are also carried out to separate the influence of the extratropics and the SST. Our results will be analysed in a mainly quantitative way to establish the importance of different timescales on the boundaries and how successful the model is in a statistical sense in reproducing the variety of observed events.

In Sect. 2 our experiments are described. A validation is presented of a 20-year run with prescribed (reanalysis) boundary conditions and standard diagnostics of the MJO are presented. In Sect. 3 diagnostics are shown from twin experiments and from experiments with mixed and time-filtered boundary conditions. Then in Sect. 4 we diagnose the temporal coherence between simulated and observed MJO events, including a consideration of ‘primary’ and ‘successive’ events as introduced in M08. Conclusions are given in Sect. 5.

2 Model runs and boundary conditions

In this study we use the Weather Research and Forecasting (WRF) regional model version 3.3.1 in a similar configuration to that used by Jourdain et al. (2011). We use a horizontal resolution of 111 km and 32 unequally spaced

vertical levels. Sub-grid scale processes are parameterised using the following schemes: the Betts–Miller–Janjic convective scheme (Betts 1986; Betts and Miller 1986; Janjic 1994); the Yonsei University planetary boundary layer (Noh et al. 2003; Hong et al. 2006) with Monin–Obukhov surface layer parameterisation; the WRF single-moment three-class microphysics scheme (Hong et al. 2004); the shortwave radiation scheme due to Dudhia (1989) and the Rapid Radiation Transfer Model (Mlawer et al. 1997) for long wave radiation. The surface drag coefficient is given by the classical Charnock (1955) relation. A prognostic sea surface skin temperature scheme (Zeng and Beljaars 2005), the Chen and Dudhia (2001) surface scheme and an annual update of the deep soil temperature are used.

The model domain is a tropical channel with boundaries at 30°N and S. At these boundaries 6-hourly data is prescribed from the National Center for Environmental Prediction (NCEP-2) reanalysis (Kanamitsu et al. 2002) for zonal and meridional wind, potential temperature, geopotential, dry air mass in column and water vapour mixing ratio. The lateral boundary conditions take the form of a boundary value specified by temporal interpolation to the reanalysis, and a zone four grid-points wide where model values are relaxed to the specified boundary values. The sea surface temperature is prescribed from daily data using the Reynolds et al. (2002) dataset, which has an effective temporal resolution of one week and so does not contribute to forcing on shorter timescales but may influence intraseasonal to interannual variability. Model integrations are carried out for the period 1993–2012. Diagnostics are carried out for the period April 1993–December 2012.

For some experiments the boundary conditions and the SSTs are subjected to temporal filtering to eliminate certain frequencies in the boundary forcing. Three different configurations are considered: standard unfiltered, designated REF; ‘notched’, designated NOTCH and ‘annual-diurnal’, designated CLIM. The NOTCH experiment borrows terminology from Gustafson and Weare (2004b), as essentially the same method is applied to our channel model. Unfiltered boundary conditions are modified by removing periods from 20–100 days. A Fourier analysis of the boundary conditions is performed and the harmonics corresponding to periods between 20 days and 92.47 days are removed. A mini taper halving the Fourier coefficients is applied for $T = 20.01$ days and $T = 91.31$ days. Diurnal and synoptic timescales remain, as does the interannual variability. In the CLIM experiment the annual cycle of the boundary conditions for the 20-year period is first calculated by averaging calendar days. The resulting 20-year repeated annual cycle is then subjected to further time filtering to remove the sub-seasonal variability associated with sampling a finite time series. All that remains is a smooth annual cycle and a diurnal cycle. The latter is retained in order to avoid damping

frequencies that may influence convection near the boundaries. The data are filtered by retaining frequencies shorter than two days, and then only the annual frequency and its harmonics at 6, 4 and 3 months. All these modifications are made to both the lateral boundary conditions and the SST. To separate these two boundary influences two ‘mixed’ experiments are carried out: REF* is a version of REF with SSTs from NOTCH; and NOTCH* is a version of NOTCH with SSTs from REF.

For each of these sets of boundary conditions (but not for mixed conditions), two 20-year runs are made. They differ only in their initial condition. The standard run (‘RUN’1) is initialised with data from 01/01/1993, and its twin run (‘RUN’2) is initialised with data from 01/01/1994. For the twin run the initial shock to the system is measurable in terms of 200 hPa mean kinetic energy, and the difference between the two runs gradually diminishes until variations around a fixed mean level are considered to represent internal variability. The timescale for the initial perturbation to die out is less than three months, so the diagnostic period of April 1993–end 2012 is unaffected by the artificial change of initial condition. Initial and boundary conditions for the complete set of experiments are presented in Table 1.

Some diagnostics to assess the global performance of the standard REF1 simulation are given in Fig. 1. The 20-year winter (November–April) mean 850 hPa zonal wind and precipitation are shown for the entire model domain compared with the NCEP2 reanalysis winds and GPCP (Adler et al. 2003) precipitation. We will concentrate on winter diagnostics throughout this paper as this is the most active period for eastward propagating MJO events, and propagating signals are more clearly identified within a given latitude range. For this study our focus is on the Indian Ocean–West Pacific region where the model reproduces the extent of the tropical westerlies from Africa out to the Pacific warm pool, although their intensity is

overestimated. Maxima in precipitation are generally well located with single intertropical and South Pacific convergence zones, although Indian ocean precipitation displays too much seasonal variation with latitude (not shown). The maximum intensity of precipitation is overestimated. The outgoing long wave radiation (OLR, not shown) has a uniform warm bias (probably associated with a tendency to trigger convection too easily) and underestimated variance, although maxima are well located as expected given the realistic placement of the precipitation maxima. Variance in lower tropospheric zonal wind (Fig. 1c, d) is stronger than observed, but is well located in the eastern Indian Ocean and across the maritime continent into the West Pacific. At least half of this variance is associated with intraseasonal (20–100 days bandpass) timescales, as is also true for the observed signal.

The propagation characteristics for convectively coupled disturbances in the winter months are depicted in Fig. 2, which shows Hovmuller correlation plots of OLR and zonal low-level wind against an equatorial OLR index in a rectangular region spanning 10N–10S and 60–90E. Note that a positive OLR anomaly corresponds to suppressed convection and thus a negative convective heating anomaly. Observed OLR is in phase quadrature with a propagating signal in the zonal wind, with enhanced convection leading westerly anomalies and following easterly anomalies. Note that strong zonal wind anomalies both precede and follow convective anomalies in time over the eastern Pacific, and this is captured in the model. As OLR correlations weaken over the eastern Pacific the dynamical signal propagates faster. This well known pattern is reproduced to some extent in the model which displays clear propagating signals in both OLR and associated zonal wind. The OLR autocorrelation diminishes too quickly with longitude although the convectively coupled dynamical signal shows essentially the same propagation characteristics as the observed signal.

In summary the model has a reasonable climatology in terms of wind and convection, and suffers from some commonplace systematic errors in its capacity to couple these phenomena in a realistic manner for propagating systems. The model represents a potentially revealing testbed for the main question posed in this article: what is the strength of the extratropical influence in initiating and maintaining these propagating systems?

3 Internal versus boundary induced variability

Having assessed the performance of the REF experiments with full lateral and SST boundary conditions, we now compare them with the filtered lateral and SST boundary condition experiments, NOTCH (intraseasonal timescales

Table 1 Summary of model experiments

EXP	Initial condition	Lateral boundary condition	SST
REF1	1/1/93	6 h unfiltered	Smoothed daily data
REF2	1/1/94		
REF*	1/1/93		20–100 days removed
NOTCH1	1/1/93	20–100 days removed	20–100 days removed
NOTCH2	1/1/94		
NOTCH*	1/1/93		Smoothed daily data
CLIM1	1/1/93	Repeated annual cycle	
CLIM2	1/1/94		

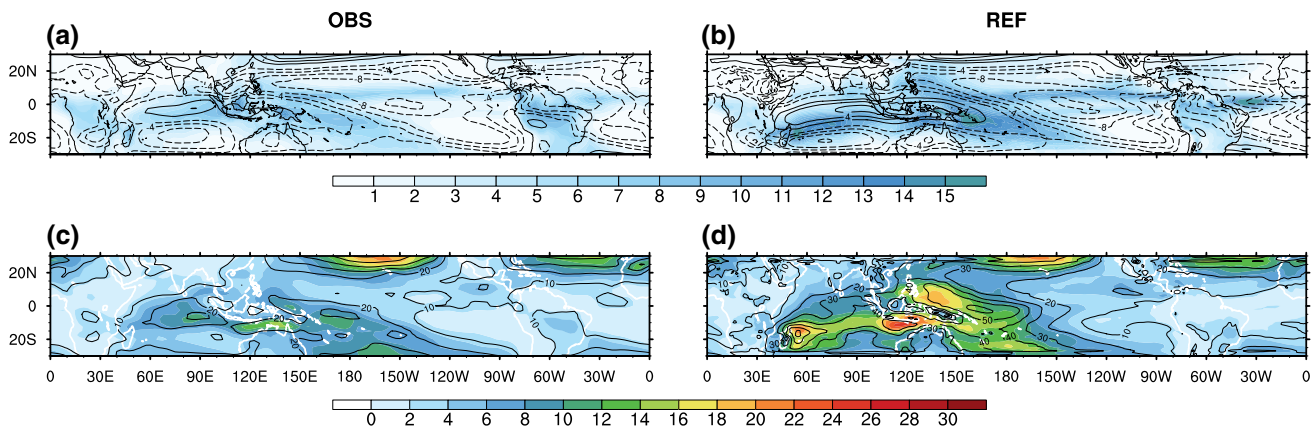


Fig. 1 Top: 20-year winter (November–April) mean 850-hPa zonal wind (contours) and precipitation (colours) for **a** observations and **b** REF1 run. The contour interval is 2 m s^{-1} for zonal wind and the units for precipitation are mm/day. The zero contour is omitted. Bot-

tom: 20-year winter (November–April) 850-hPa zonal wind total variance (contours) and intraseasonal variance (colours) for **c** observations and **d** REF1 run. Contour interval is $10 \text{ m}^2 \text{ s}^{-2}$ for total variance and $2 \text{ m}^2 \text{ s}^{-2}$ for intraseasonal variance

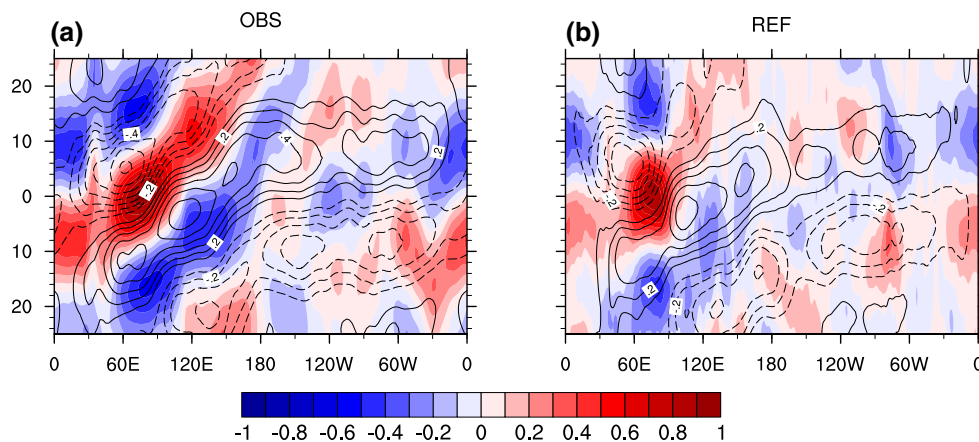


Fig. 2 Winter (November–April) lag-longitude correlation coefficients for 10°N – 10°S -averaged intraseasonal OLR (colours) and intraseasonal 850-hPa zonal wind (contours) against intraseasonal

OLR in the box 10°N – 10°S , 60° – 90°E for **a** observations and **b** REF1 run. The ordinate is lag in days from -25 to 25 . Contours and colours are plotted every 0.1 . The zero contour is omitted

removed) and CLIM (repeated annual cycle imposed). Figure 3 shows the winter mean state from these experiments for zonal wind and precipitation as in Fig. 1a, b. The NOTCH1 run is very similar to the REF1 run in all respects. The biggest differences in the climatology are close to the boundaries. There is also a weakening of the Indian Ocean equatorial westerlies and of the precipitation on their southern flank. The spatial distribution is, however, very similar and the mean state has clearly not been affected much by removing intraseasonal variations from the boundary conditions. The result for the CLIM1 run is very different with major departures in the positions of the rain bands and the westerlies and large changes near the boundaries. These results are consistent with those of Ray and Li (2013) and Ding and Kuang (2016) who attributed

errors in their climatology in similarly constrained GCM runs to missing momentum fluxes from extratropical synoptic scale transients. The interest in retaining the CLIM runs lies in the fact that there is strictly no sub-seasonal influence from the boundaries so they serve as a test case for evaluating the proportion of internal variability in the tropics.

In our experimental setup, there are two types of comparison to be made. Firstly results with different time filtering on the boundaries can be compared, with the caveat that in the CLIM runs the underlying climatology is different so the differences we see in the variance and propagation characteristics might not be directly due to the boundary influences on the timescales considered. Secondly results from twin experiments can be examined to give a clean

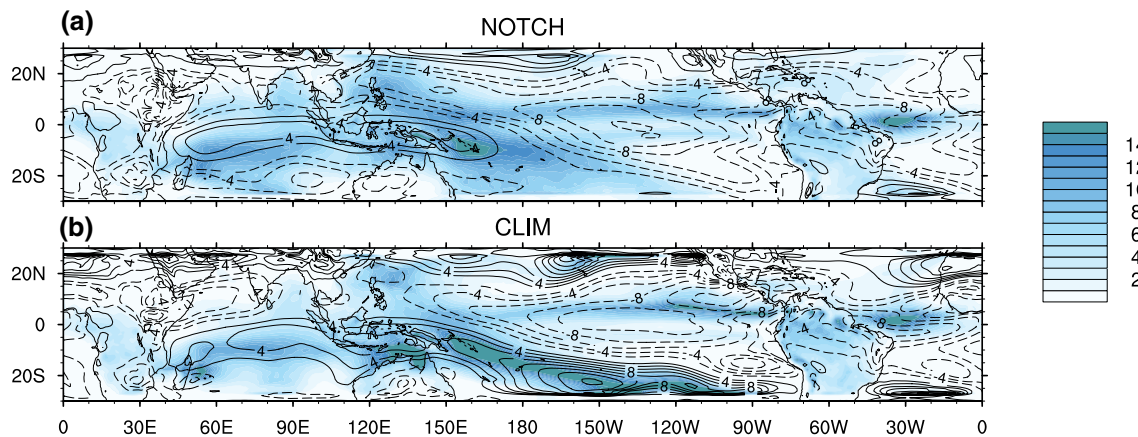


Fig. 3 20-year winter (November–April) mean 850-hPa zonal wind (*contours*) and precipitation (*colours*) for **a** NOTCH1 run and **b** CLIM1 run. *Contours and colour scales as in Fig. 1 (a, b)*

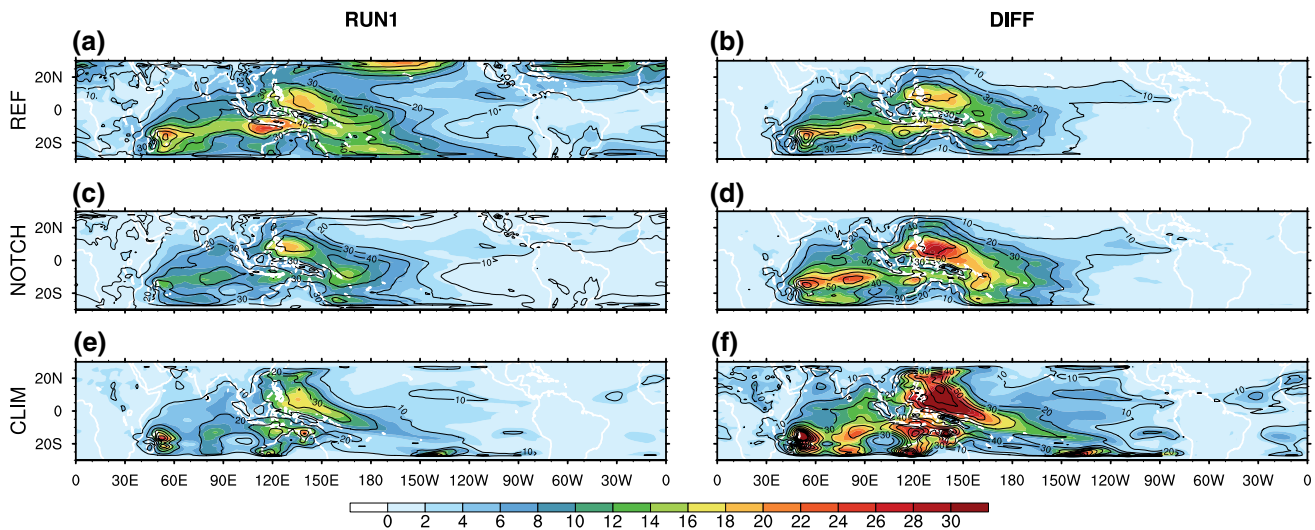


Fig. 4 20-year winter (November–April) 850-hPa zonal wind total variance (*contours*) and intraseasonal variance (*colours*) for each set of runs: *first row a, b* REF1, *second row c, d* NOTCH1 and *third row e, f* CLIM1. *First column (a, c, e) shows the variance of a standard*

run and second column (b, d, f) shows the variance of the difference between twin runs. Contour interval is $10 \text{ m}^2\text{s}^{-2}$ for total variance and $2 \text{ m}^2\text{s}^{-2}$ for intraseasonal variance. The zero contour is omitted

assessment of internal versus boundary-induced variability for a given set of boundary conditions. The results from the two approaches are shown together in Fig. 4. The first column shows the winter variance of 850 hPa zonal wind from the standard runs for REF, NOTCH and CLIM boundary conditions. Variance from the twin runs (not shown) is in all cases almost identical to the variance from the corresponding standard run. It is clear that the boundary conditions have a marked effect on the variance. Although its climatology is very similar, the intraseasonal variance in the NOTCH1 run is reduced by about half, consistent with the removal of intraseasonal timescales from the boundaries. The total variance is correspondingly reduced. Maxima in

variance retain their positions compared to the REF1 run, as might be expected in a model with a similar mean state (the exception is the northern boundary maximum, which has unsurprisingly disappeared). The reduced variance in the NOTCH1 run amounts to circumstantial evidence that the intraseasonal boundary signal is important in generating intraseasonal variance in the model domain. The CLIM1 run shows similarly reduced variance maxima, but in this case the spatial distribution is also substantially altered and less realistic, consistent with the degraded mean state.

The second column of Fig. 4 shows the variance of the difference between the standard and twin runs. This provides an independent check on the importance of the

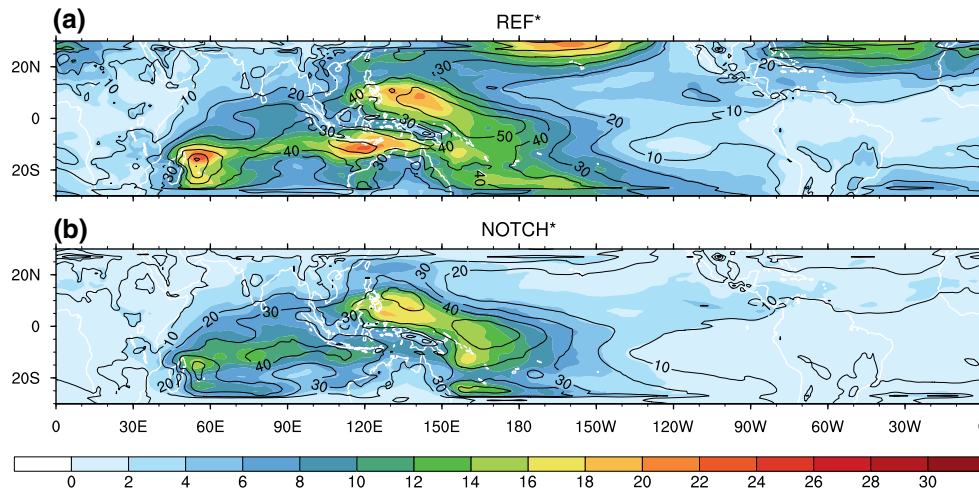


Fig. 5 20-year winter (November–April) 850-hPa zonal wind total variance (contours) and intraseasonal variance (colours) for runs with mixed boundary conditions. **a** *REF** lateral boundary conditions from

REF and SSTs from *NOTCH*. **b** *NOTCH** lateral boundary conditions from *NOTCH* and SSTs from *REF*. Contours and colour scales as in Fig. 4

boundary signal. After a spinup period, we expect the twin runs to be independent of their initial conditions, but influenced by their identical boundaries. The variance of the difference between the runs thus gives a measure of the part of the variance that is independent of the boundaries. It is of course zero on the boundary, where the two runs are identical, but will in general have a value of $\text{var}(\text{RUN1}) + \text{var}(\text{RUN2}) - 2 \times \text{covar}(\text{RUN1}, \text{RUN2})$. So the range of possible values is from zero, if the integrations are perfectly correlated, to $4 \times \text{var}(\text{RUN1})$, if they are perfectly anticorrelated. If *RUN1* and *RUN2* are independent, then their covariance will be zero and the variance of the difference will be twice the variance of an individual run. Clearly the two runs are not independent because they are affected by their identical boundary conditions, and thus will probably have a positive covariance. So we expect to see values less than $2 \times \text{var}(\text{RUN1})$ for the variance of the difference.

Looking first at the *REF* runs, the variance of the difference between twin runs is of about the same magnitude as the variance of an individual run, with similarly positioned maxima. This implies that the boundaries play an important role in the model's intraseasonal variability, accounting for about half the intraseasonal variance. This picture changes radically when we remove the intraseasonal signal from the boundary conditions. The variance of the difference for the *NOTCH* runs is close to double the individual variance over much of the domain and the spatial distribution is again similar. This also holds for the *CLIM* runs, where we expect the variability to be predominantly internal. The variance of the difference is again approximately double the individual value and the spatial distribution mimics very closely the considerably altered signal associated with the modified mean state.

It is pertinent at this point to ask to what extent these changes in variance are due to the extratropics or to the SST, as both boundary conditions are altered together in the experiments shown so far. Figure 5 shows results from the *REF** and *NOTCH** runs with mixed boundary conditions. The *REF** run has intraseasonal variance on the lateral boundaries but not in the SSTs. The *NOTCH** run has intraseasonal variance in the SSTs but not on the lateral boundaries. It can be readily seen that *REF** is similar to *REF1* and *NOTCH** is similar to *NOTCH1*. So in terms of the magnitude of low-level zonal wind variance, it is fairly clear that the tropical SSTs play a minor role compared to the lateral boundaries.

Our results for the intraseasonal variance indicate that intraseasonal boundary forcing has an important influence, but that the spatial form of the variance in all cases is essentially dictated by the model's time-mean state. Internal variance has a similar pattern to the full signal. It appears that although the boundary forcing is important in determining the magnitude of the variance, it has little influence on the structure and positioning of intraseasonal signals closer to the equator. One might hypothesise that the extratropical signal serves to trigger modes of variability that are internal to the tropics and thereby increase tropical variance.

It remains to assess the propagation characteristics of the simulations and the degree of convective coupling in the dynamical signal. The MJO is essentially a convective signal and the following analysis will concentrate on dynamical signals that are coupled to convective activity in the Indian Ocean region, as isolated in Fig. 2. Although the convective signal itself shows limited propagation in the model, the associated low level zonal winds do show some variation from one experiment to another in their

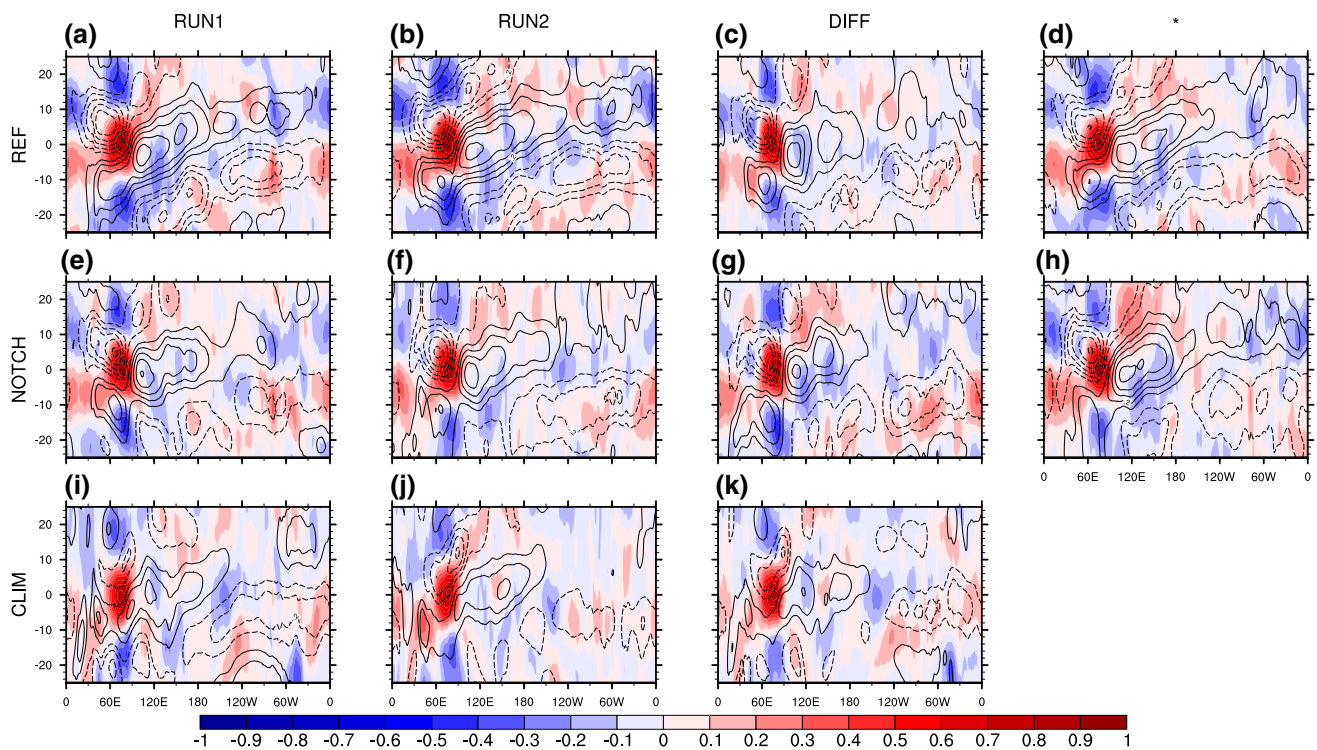


Fig. 6 Winter (November–April) lag-longitude correlation coefficients for 10°N – 10°S -averaged intraseasonal OLR (colours) and intraseasonal 850-hPa zonal wind (contours) against intraseasonal OLR in the box 10°N – 10°S , 60° – 90°E for each set of runs. *First row a, b, c, d REF*; *second row e, f, g, h NOTCH* and *third row i, j, k CLIM*. *First column (a, e, i) shows standard runs: REF1, NOTCH1,*

CLIM1, second column (b, f, j) shows the twin runs: REF2, NOTCH2, CLIM2 and third column (c, g, k) shows the correlations for the difference between twin runs. The last column (d, h) shows the mixed boundary condition experiments REF and NOTCH* respectively. The ordinate is lag in days from –25 to 25. Contours and colours are plotted every 0.1. The zero contour is omitted*

propagation characteristics. Figure 6 shows correlation Hovmullers for the whole suite of experiments, including the twin runs and the mixed runs. The degree of similarity between the first two columns indicates the robustness of our results for each set of boundary conditions. The third column shows the correlation for the difference between the two runs, as before, a signal independent of the boundary conditions. Compared to all the other diagnostics, the REF runs show stronger propagation in both the downstream response and upstream precursors of a maximum in OLR. The plot based on the difference between the REF runs shows a weaker remote signal with no clear sense of propagation. The same can be said to some degree for the NOTCH experiments, in which there is less distinction between the individual runs and the diagnostics based on the difference between them. Our two separate ways of evaluating the importance of the extratropical influence thus give similar results: weaker propagation, implying a role for the extratropical intraseasonal signal. The CLIM runs show particularly weak and distorted signals with no robust evidence of propagation in the dynamical fields associated with convection. As for the mixed boundary condition experiments, the REF* run, with full lateral but

filtered SST boundary conditions, shows weaker wind-field precursors than either of the pure REF runs, suggesting a potential triggering role for the SSTs when considering convectively coupled signals exclusively. However, this does not translate into stronger precursors in the NOTCH* run (full SST but filtered lateral boundary conditions), implying that the extratropical influence is still an essential element.

The Hovmuller diagrams in Figs. 2 and 6 give limited information about the structure of propagating signals, so to better illustrate the typical form of disturbances crossing the Indo-Pacific region Fig. 7 shows a series of lagged one-point correlation maps, referenced to OLR in the same rectangular region spanning 10°N – 10°S and 60° – 90°E . Values of cross-correlation for the intraseasonal (20–100 day) signal are shown for the model domain with lags from –25 days to 25 days. REF1, NOTCH1 and associated mixed boundary condition runs are compared with observations.

Observed convective anomalies propagate at MJO timescales and the divergent wind on the equator propagates with them. Convective heating is associated with enhanced westerlies to the west and easterly anomalies to the east. Westerly perturbations in the Indian Ocean on

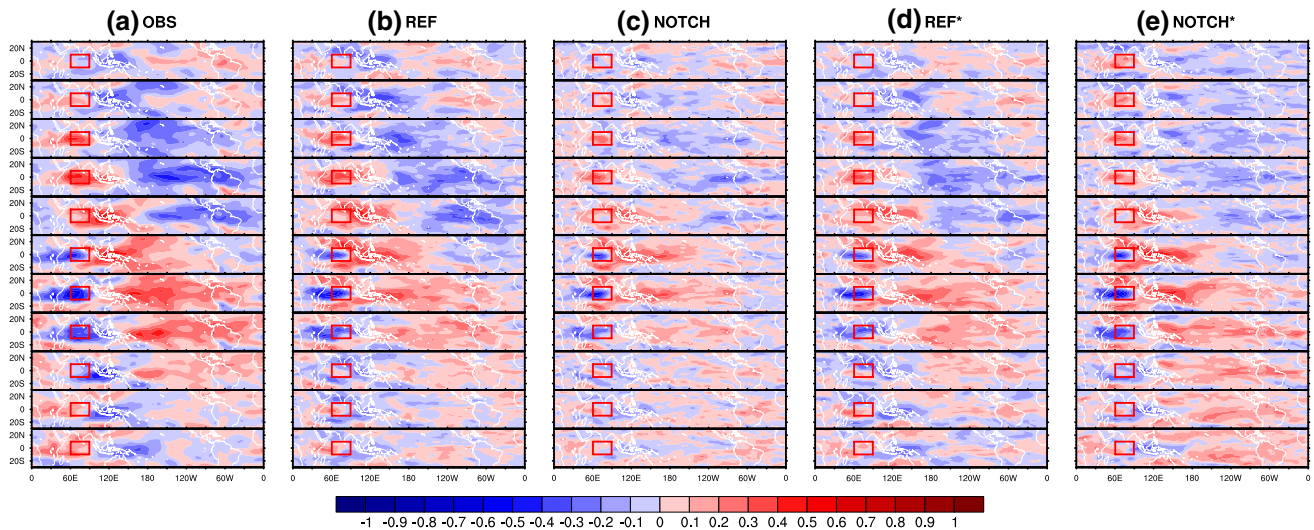


Fig. 7 Winter (November–April) intraseasonal 850-hPa zonal wind anomalies correlated against intraseasonal OLR in the box 10°N – 10°S , 60° – 90°E for different lags from -25 days to $+25$ days every 5

days going down the column, for: **a** observations **b** REF1 **c** NOTCH1 **d** REF* and **e** NOTCH* runs. Colours are plotted every 0.1

these timescales are associated with a tropical wavenumber one pattern with a maximum easterly anomaly over the West Pacific. The eastward propagation of the MJO signal is seen in the observed low level wind around the globe with a transit timescale of about 40 days and a signature of slower propagation in the Indo-Pacific region. Precursors in the low level wind can be identified over the mid-Pacific 10–15 days beforehand, and are seen to cross the Atlantic and Africa before strongly coupling with convection in the Indo-Pacific sector. The structure at the correlation point is more confined in latitude and resembles a double Rossby gyre response to an on-equator convective heating anomaly.

A similar precursor signature is seen in REF1, although the subsequent coupling to convection is weaker as already discussed. In comparison, the NOTCH1 run has somewhat weaker remote correlations and the signature of propagation is not as clear. Precursors are more equatorially confined as if limited to an equatorial Kelvin wave (a trait shared with the CLIM runs, not shown). It is interesting that the strongest upstream correlations are in the Pacific region although without further experiments this does not allow us to attribute causal significance to this region. All these results can be contrasted with the uncoupled dynamical signals (autocorrelation of the zonal wind) which also display eastward propagating large scale signals (not shown), but without convective coupling the NOTCH1 run shows similar correlation patterns to the REF1 run. It is the part of the signal that is coupled to convection that appears to be more dependent on the boundary conditions. Removing intraseasonal variance from the SST (the REF* run) makes little difference to the REF result, although consistent with

Fig. 6 there is a slight reduction in correlation with precursors in the eastern Pacific. Adding intraseasonal SST variance back into the NOTCH experiment (the NOTCH* run) does not make much difference either. In fact the difference between NOTCH* and NOTCH1 is no greater than the difference between NOTCH1 and NOTCH2 (not shown). So there is no clear evidence here for a systematic independent role for the SSTs. We will, however take up this matter in the next section.

4 Temporal coherence with the observed extratropics

In the previous section we presented composite evidence for the importance of the extratropics and found that in general the presence of an intraseasonal signal on the boundaries boosts the magnitude of intraseasonal variance in the eastern hemisphere equatorial region. Convectively coupled propagating signals in the model originate at least in part from boundary variance, and appear about 15 days prior to Indian-Ocean convection as low-level zonal wind anomalies in the Pacific.

Although these covariance statistics can point to evidence of systematic behaviour, they do not address the fact that the MJO is an irregular phenomenon, best described as a sequence of events. Individual Madden-Julian events can be characterised according to their potential predictability, and this might be linked to their connections with the extratropics. The advantage of using a regional model, compared to a free-running GCM, is that the entire integration is tied to the observed realisation. Model dates correspond to real

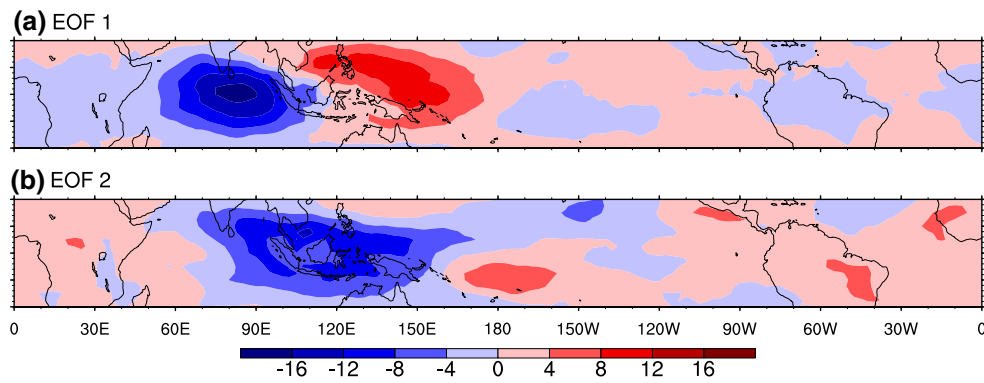


Fig. 8 **a** EOF1 and **b** EOF2 of intraseasonal OLR scaled by one standard deviation. Contour interval is 4 W m^{-2}

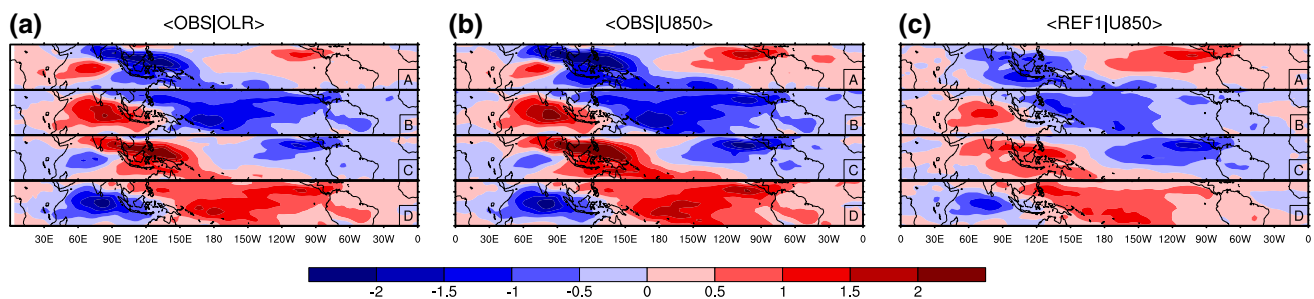


Fig. 9 Intraseasonal 850-hPa zonal wind anomaly composites for phases *A*, *B*, *C* and *D* as indicated in *bottom right box* of each plot. **a** Composites calculated from time series of observed OLR-based

phases. **b** reanalysis u850-based phases. **c** model u850 (REF1 run) phases. Contour interval is 0.5 m s^{-1}

dates and the model simulation is linked to the observed time sequence through the influence of the boundaries.

One of the conclusions from the work of M08 was that it is the so called ‘successive’ events that are linked to the extratropics. This suggests that ‘primary’ events are internal to the tropics, and that they influence the extratropics which in turn feed back on the tropics to initiate successive events. This category of events may therefore be interesting to isolate and compare with primary events in terms of model performance. How well do the events simulated in the model correspond in time to real events? Is there any difference in the model’s capacity to reproduce successive events compared to primary events? If successive events are boundary influenced, one would expect them to be present at the right time in the model simulation. If primary events arise from internal variability one might expect them to be perhaps present in the model, but not synchronised with observed primary events. In this section some diagnostics and simple skill scores are presented to give a quantitative answer to these questions.

First, following M08, a sequence of MJO phases was derived from the observed OLR. Empirical orthogonal functions were calculated from 20–100-day filtered data over the integration period. The first two EOFs are shown

in Fig. 8. They account for 8.5 and 6.8 % of the variance. Their spatial structure corresponds to enhanced convection over the Indian Ocean and the Indonesian region respectively and resembles very closely that shown in M08 (see his Fig. 1) and in the recent study by Kiladis et al. (2014). A phase index: *A*, *B*, *C*, *D*, was assigned to each day in the filtered data depending on whether its principal components resolved into quadrants centred on EOF1, EOF2, -EOF1, -EOF2 respectively. An *N* phase was also defined for cases where the magnitude of the projection (normalised by the variance) was less than a threshold level, which was set at 0.65. In fact, to avoid multiple transitions near this circular boundary we followed the same procedure as M08 and defined a buffer zone such that an *N* phase begins when the projection falls below 0.55 and ends when it exceeds 0.75.

The next step is to compare these phases with the model integrations. Given the documented systematic errors of the model in simulating propagating convective disturbances, it is preferable to define a metric using the 850 hPa zonal wind rather than the OLR, while at the same time isolating the convectively coupled aspect of the observed dynamical signal. To do this we start with the reanalysis wind. Observed u850 composites are calculated based on the ABCD phases deduced from the OLR. These are shown in

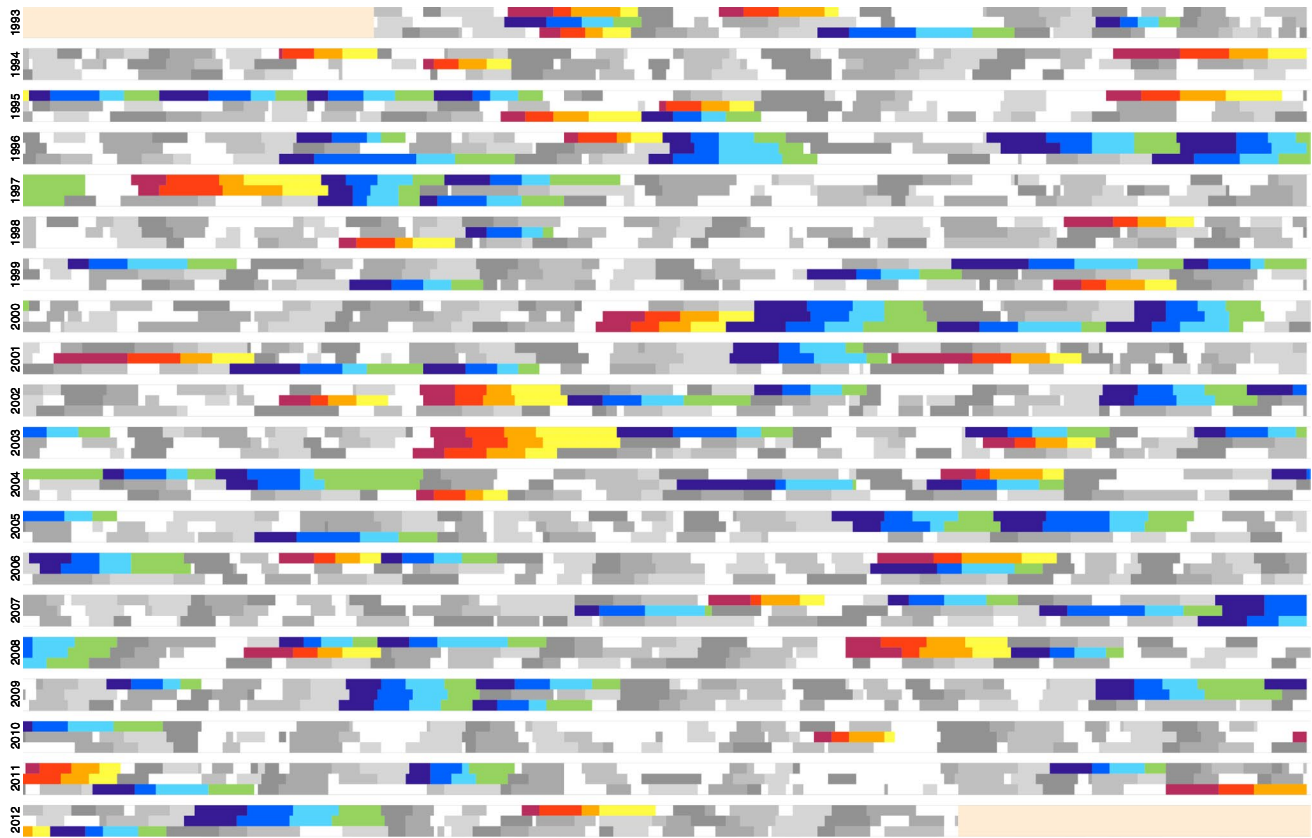


Fig. 10 Twenty years of diagnosed MJO phases (ABCD and N). For each year the first row is based on observed OLR, the second row reanalysis u850 and the third row model u850 (REF1). Shades of grey indicate different phases: *darkest* for A to *lightest* for D. Periods designated N where no MJO phase is active are *not shaded*. Complete

uninterrupted ABCD sequences are *coloured* if they are preceded by an N phase (primary events: *red-yellow*) or by a D phase (successive events: *blue-green*). First and last years are truncated due to band-pass filtering

Fig. 9a, and clearly denote the eastward propagating low-level convergence zone associated with the MJO. It is these dynamical patterns that will form the basis for comparison with the model. Before this can be done, a new timeseries of phases associated with the observed low level zonal wind must be created. Daily fields from the 20–100-day filtered reanalysis are compared with the four u850 composites. Each day is assigned a phase corresponding to the strongest projection, creating a daily sequence of phases ABCD. A criterion is added that the projection must exceed a threshold, set at 0.2, otherwise an N phase is assigned. The new sequence of phases, ABCDN is not identical to the sequence calculated from the OLR data, but it is this new sequence that is relevant for subsequent comparison with model simulated winds. Figure 9b shows composite reanalysis winds calculated from the new phase sequence. They are unsurprisingly extremely similar to the original composites.

We now repeat this procedure with the model results. A model-generated sequence of phases using the REF1 run produces the composite structures shown in Fig. 9c. This

confirms that the model-generated winds that project onto the observed wind patterns associated with the four OLR-derived phases (Fig. 9a) have detailed spatial structures that closely resemble the equivalent composites made with the reanalysed winds (Fig. 9b) although Indian Ocean convergence and divergence during active (A) and suppressed (C) phases respectively is under-represented in the model.

More interesting than the similarity of the composites is the coherence of the time sequences. To what extent does the model reproduce the phase sequences in the reanalysis winds? Figure 10 shows a graphic representation of the entire 20-year timeseries with four lightening shades of grey for the A, B, C and D phases respectively (N phases are not shaded). For each year, the three lines show the original phases based on OLR, the phases constructed with reanalysis winds and the phases using model winds from the REF1 experiment. Episodes of cyclic behaviour with a predominant ABCD sequence are apparent (most complete sequences are coloured, as explained below). The correspondence between the three sequences in Fig. 10 depends to some extent on the values chosen for the two thresholds

Table 2 Percentage of success in reproducing observed u850 phases compared to chance (Monte-Carlo simulations in parentheses) for 1) phase; 2) event and 3) active phase given that there is an event

EXP	1: ABCDN	2: N or not N	3: ABCD given not N
REF1	38.8 (20.6)	70.5 (65.8)	49.7 (25.5)
REF2	38.4 (20.4)	69.6 (65.5)	50.1 (25.5)
REF*	33.5 (20.3)	66.2 (63.8)	45.0 (25.3)
REFdiff	21.1 (20.3)	59.9 (59.6)	26.9 (25.5)
NOTCH1	23.9 (20.3)	63.5 (63.7)	31.6 (25.1)
NOTCH2	21.4 (20.1)	62.4 (62.8)	27.7 (25.0)
NOTCH*	29.3 (20.1)	67.0 (66.7)	39.6 (25.1)
NOTCHdiff	18.3 (19.9)	61.5 (62.0)	22.4 (24.8)
CLIM1	21.5 (20.2)	59.7 (59.7)	27.4 (24.9)
CLIM2	21.3 (20.1)	57.3 (57.4)	27.7 (25.1)
CLIMdiff	19.6 (19.9)	58.5 (59.4)	25.3 (24.7)

that define the N phases. For the first threshold used on the OLR data we chose a value of 0.65 that delivers about 20 % N, so it is roughly as common as A, B, C and D. Given this choice, the second threshold was set at 0.2 to maximise correspondence between observed OLR and wind phases, whilst retaining a similar proportion of N cases. It turns out that this choice actually comes close to minimising the correspondence between model and reanalysis, but this is desirable because improved correspondence scores from threshold tuning are mostly trivial results based on simple probabilities (if everything is N, or if there is no N, a better result can be had by chance). Within a reasonable range, the choice of thresholds does not affect the conclusions discussed below.

With a phase occupation timeseries for each model run, a number of questions can be framed. A measure of hind-cast skill can be devised for each of these questions based on how often the model timeseries produces the same phase as the reanalysis. The specification of this ‘skill score’ is given in parentheses, together with the associated probability from simple chance assuming equal proportions for the phases.

- (1) How good is the general correspondence of phases? (%ABCDN cf 20 %)
- (2) How well does the model discriminate the existence of MJO events regardless of phase? (%(not N) + %N cf 68 %)
- (3) given that there is an MJO event in both sequences, how well do the phases correspond? (%ABCD cf 25 %)

These three skill scores are given in Table 2 for all eleven experiments: i.e. twin runs for REF, NOTCH and CLIM; results for the differences between twins and results for the two mixed boundary condition runs REF* and NOTCH*

(see Table 1 for a reminder of the boundary conditions). Shown in parentheses next to each score are results from Monte-Carlo simulations, where daily phase categories from the reanalysis have had their year scrambled but retain the same calendar date. One thousand such calculations were performed for each experiment. This gives a measure of the null hypothesis taking into account unequal distributions between phases and between model and observations. Values are similar to the simple probabilities given in the list above. The standard deviations of the Monte-Carlo tests are typically of the order of 0.5, 0.4 and 0.7 for tests 1–3 respectively, giving a measure of significance for results that exceed this baseline score. The results in Table 2 clearly identify the two REF runs as having significant skill in matching observed episodes of the MJO, and in reproducing the correct phase. The REF runs stand out from the baseline random expectation in all three scores. In particular, the REF runs have skill in identifying events (question 2).

Among the other runs, the only ones that perform significantly better than chance at identifying events are the two mixed boundary condition runs. The REF* experiment (full lateral boundary conditions but filtered SSTs) is almost as good as REF1 and REF2. The NOTCH* experiment (full SSTs but filtered lateral boundary conditions) is better than NOTCH1 and NOTCH2, but not significantly so. Thus it appears that information on intraseasonal timescales from the extratropics, and possibly the SST can provide some degree of skill for triggering events. None of the other runs show any skill in identifying events although there are some examples of skill in questions 1 and 3, doubtless associated with correct phase sequencing, which is to be expected even for purely internally generated propagating patterns. We can draw a very clear conclusion that intraseasonal boundary signals play a role in the timing of episodic MJO events in the simulation. We can also conclude that these boundary signals can be a source of model skill whether they come from the extratropics or from the SST, although we have not demonstrated that these two sources of information from the observations are independent from one another.

Shown in Table 3 are statistics for primary and successive events. Primary events are defined as full ABCD sequences that are preceded by N. These are shown with warm red-to-yellow colours in Fig. 10. Successive events are full ABCD sequences that are preceded by D (as in M08, we focus on the Indian Ocean as a starting point). These are shown with cold blue-to-green colours in Fig. 10. Note that successive events are not always preceded by primary events because for an ‘event’ to be counted it must be a complete sequence. Based on observed OLR there are 17 primary and 41 successive events for our threshold criterion. Observed winds identify 14 primary and 28 successive events. The REF runs have fewer events and the

Table 3 Hindcast success rates for primary and successive events deduced from observed u850

EXP	Primary			Successive		
	Hit	Miss	FA	Hit	Miss	FA
REF1	2	12	6	7	21	12
REF2	2	12	6	9	19	9
REF*	1	13	5	6	22	10
REFdiff	1	13	2	0	28	3
NOTCH1	2	12	8	0	28	8
NOTCH2	1	13	8	3	25	7
NOTCH*	1	13	10	5	23	5
NOTCHdiff	2	12	7	2	26	4
CLIM1	0	14	9	1	27	7
CLIM2	2	12	6	3	25	8
CLIMdiff	1	13	4	2	26	8

proportion of primary events is slightly lower. These model events are classified as ‘hits’ if there is at least one day in common with the observed dataset regardless of phase, or ‘false alarms’ if there is not. An observed event that is not captured by the model is counted as a ‘miss’. The number of hits is very low for primary events, and still quite low for successive events although the success rate is improved. REF experiments perform better than NOTCH, CLIM or DIFF experiments for successive events, and again there is an indication that the mixed boundary conditions give improved skill compared to NOTCH boundary conditions. The false alarms outnumber the hits in all cases, but especially for primary events. This is consistent with our expectation that primary events are associated with tropical internal variability whereas successive events can be influenced by the extratropics. However, the number of misses dominates, showing poor model skill overall.

5 Conclusions

The results presented in this paper can be discussed from two viewpoints: partitioning of variance and attribution of cause. In order to address the former, we have analysed long enough runs to be able to make general statements, and we have designed experiments that isolate different sources of variability. Experiments have been performed to partition the variance associated with boundary influences from the internally generated variance. The conclusions are quite clear, at least in terms of the modelling framework used here.

- Tropical intraseasonal propagating signals are present to more or less the same degree of realism in all simulations in which the mean state is well represented. We can interpret the structure and propagation characteristics of these signals as internal to the tropics.

- A large fraction of the intraseasonal variance associated with propagating tropical signals is provided by boundary influence on the same, intraseasonal timescale. This boundary influence does not change the structure of the variance, only its magnitude, suggesting a triggering role for the extratropics that stimulates heightened activity for internal tropical modes.
- In terms of generating variance in the model experiments, intraseasonal variability in SSTs is of secondary importance compared to the signal coming from the lateral boundaries.
- There is no evidence of faster (<20 days) transients on the boundaries having a direct effect on the magnitude of tropical intraseasonal variance. These transients are, however, indispensable for a faithful simulation of the tropical mean state, which in turn influences the structure of tropical intraseasonal variance. This result is consistent with the conclusions of Ray and Li (2013) but differs from the findings of Vitart and Jung (2010) who implicate extratropical synoptic transients in the initiation of MJO events. Their experimental design is somewhat different to ours, based on the effect of relaxation on ensemble hindcasts, but further study is needed to interpret the potential interaction of timescales.

Although the conclusions derived from the partitioning of model variance are quite convincing, they cannot formally allow an attribution of cause. The possibility that the boundaries might reintroduce an observed signal of tropical origin into the simulated tropics remains an important caveat when interpreting these experiments in terms of extratropical influence. In our experiments, regressions and composites were used to try and identify systematic precursor signals associated with boundary influence. From the diagnostics shown here there is a suggestion of a role for precursors in the Pacific sector that propagate within the

tropics to trigger convective events in the Indian Ocean. The Pacific sector is a favoured region for Rossby wave penetration into the tropics. In our simulations, boundary-induced precursors appear to have origins that are well separated in both time and longitude from MJO events in the Indo-Pacific region. This lends credence to the idea that these results are not merely an artifact of regional MJO signals influencing local boundary values. However, in order to test this conclusion, further work is needed to diagnose the longitude of greatest influence and to trace boundary influences back to extratropical flow anomalies.

Another way to investigate the attribution problem is by testing predictability, and for this part of the study some basic measures of hindcast skill were introduced. The statistics for the number of Madden–Julian events in the model that coincide with observed events reveals a significant influence for the boundaries. The hindcast skill of the model in reproducing ‘primary’ and ‘successive’ events matches our expectations, and the hit rate is clearly better in the REF runs where there is intraseasonal boundary influence, at least for successive events (although there are still many misses and false alarms). For this measure, which directly compares model events with observed realisations, it appears that intraseasonal SST variability may also be a source of hindcast skill. Assessing the independence of these two factors, and deducing a pathway for extratropical influence is a potential area for future work with coupled atmosphere–ocean integrations.

Although the lack of skill may be an inevitable consequence of the large fraction of internally generated variance, the model skill could possibly be improved by reducing the common systematic error in its representation of propagating organised convection. Interestingly, the role of the boundaries is better isolated when concentrating on convectively coupled disturbances. Just looking at the dynamics alone is less discriminating. So perhaps an improvement in the model’s representation of convection would lead to an improvement in its representation of boundary influence. Improvements in this aspect of the simulation may open the door to further useful diagnostic studies focussed on attribution, precursors and forecasting.

Acknowledgments We thank the two anonymous reviewers for suggestions that helped improve the clarity and pertinence of the manuscript. Severin Thibaut was supported by a grant from the french ministry of research and higher education. Model integrations were performed using HPC resources from CALMIP computing centre, Toulouse.

References

- Adames AF, Patoux J, Foster RC (2014) The contribution of extratropical waves to the MJO wind field. *J Atmos Sci* 71:155–176
- Adler RF, Huffman GJ, Chang A, Ferraro R, Xie PP, Janowiak J, Rudolf B, Schneider U, Curtis S, Bolvin D et al (2003) The version-2 global precipitation climatology project (gpcp) monthly precipitation analysis (1979–present). *J Hydrometeorol* 4(6):1147–1167
- Bellenger H, Duvel JP (2007) Intraseasonal convective perturbations related to the seasonal march of the Indo-Pacific monsoons. *J Clim* 20:2853–2863
- Betts AK (1986) A new convective adjustment scheme. Part I: observational and theoretical basis. *Q J Roy Meteorol Soc* 112(473):677–691
- Betts A, Miller M (1986) A new convective adjustment scheme. Part II: single column tests using gate wave, bomex, atex and arctic air-mass data sets. *Q J Roy Meteorol Soc* 112(473):693–709
- Charnock H (1955) Wind stress on a water surface. *Q J Roy Meteorol Soc* 81(350):639–640
- Chen F, Dudhia J (2001) Coupling an advanced land surface–hydrology model with the penn state–near mm5 modeling system. Part I: model implementation and sensitivity. *Mon Weather Rev* 129(4):569–585
- Crueger T, Stevens B, Brokopf R (2013) The Madden–Julian oscillation in echam6 and the introduction of an objective mjo metric. *J Clim* 26(10):3241–3257
- Dias J, Leroux S, Tulich S, Kiladis G (2013) How systematic is organized tropical convection within the mjo? *Geophys Res Lett* 40(7):1420–1425
- Ding M, Kuang Z (2016) A mechanism-denial study on the madden–julian oscillation with reduced interference from mean state changes. *Geophys Res Lett* 43 (doi:10.1002/2016GL06772.)
- Dudhia J (1989) Numerical study of convection observed during the winter monsoon experiment using a mesoscale two-dimensional model. *J Atmos Sci* 46(20):3077–3107
- Ferranti L, Palmer T, Molteni F, Klinker E (1990) Tropical–extratropical interaction associated with the 30–60 days oscillation and its impact on medium and extended range prediction. *J Atmos Sci* 47(18):2177–2199
- Flatau MK, Flatau PJ, Rudnick D (2001) The dynamics of double monsoon onsets. *J Clim* 14(21):4130–4146
- Flatau MK, Flatau PJ, Schmidt J, Kiladis GN (2003) Delayed onset of the 2002 Indian monsoon. *Geophys Res Lett* 30(14):1768. doi:10.1029/2003GL017434
- Frederiksen JS (2002) Genesis of intraseasonal oscillations and equatorial waves. *J Atmos Sci* 59(19):2761–2781
- Frederiksen J, Frederiksen C (1997) Mechanisms of the formation of intraseasonal oscillations and australian monsoon disturbances: the roles of convection, barotropic and baroclinic instability. *Contrib Atmos Phys* 70(1):39–56
- Frederiksen JS, Lin H (2013) Tropical–extratropical interactions of intraseasonal oscillations. *J Atmos Sci* 70(10):3180–3197
- Gustafson WI, Weare BC (2004a) Mm5 modeling of the Madden–Julian oscillation in the Indian and West Pacific Oceans: -model description and control run results. *J Clim* 17(6):1320–1337
- Gustafson WI, Weare BC (2004b) Mm5 modeling of the Madden–Julian oscillation in the Indian and west Pacific Oceans: implications of 30–70-day boundary effects on mjo development. *J Clim* 17(6):1338–1351
- Hendon HH, Liebmann B, Newman M, Glick JD, Schemm J (2000) Medium-range forecast errors associated with active episodes of the Madden–Julian oscillation. *Mon Weather Rev* 128(1):69–86
- Hendon HH, Salby ML (1994) The life cycle of the Madden–Julian oscillation. *J Atmos Sci* 51(15):2225–2237
- Hong SY, Dudhia J, Chen SH (2004) A revised approach to ice microphysical processes for the bulk parameterization of clouds and precipitation. *Mon Weather Rev* 132(1):103–120
- Hong SY, Noh Y, Dudhia J (2006) A new vertical diffusion package with an explicit treatment of entrainment processes. *Mon Weather Rev* 134(9):2318–2341

- Hoskins BJ, Yang G (2000) The equatorial response to higher-latitude forcing. *J Atmos Sci* 57:1197–1213
- Hsu HH, Hoskins BJ, Jin FF (1990) The 1985/1986 intraseasonal oscillation and the role of the extratropics. *J Atmos Sci* 47(7):823–839
- Hung MP, Lin JL, Wang W, Kim D, Shinoda T, Weaver SJ (2013) Mjo and convectively coupled equatorial waves simulated by cmip5 climate models. *J Clim* 26(17):6185–6214
- Inness PM, Slingo JM (2003) Simulation of the Madden–Julian oscillation in a coupled general circulation model. Part I: comparison with observations and an atmosphere-only gcm. *J Clim* 16(3):345–364
- Janjic ZI (1994) The step-mountain eta coordinate model: further developments of the convection, viscous sublayer, and turbulence closure schemes. *Mon Weather Rev* 122(5):927–945
- Jourdain NC, Marchesio P, Menkes CE, Lefevre J, Vincent EM, Lengaigne M, Chauvin F (2011) Mesoscale simulation of tropical cyclones in the South Pacific: climatology and interannual variability. *J Clim* 24(1):3–25
- Jung T, Palmer T, Rodwell M, Serrar S (2010) Understanding the anomalously cold European winter of 2005/2006 using relaxation experiments. *Mon Weather Rev* 138(8):3157–3174
- Kanamitsu M, Ebisuzaki W, Woollen J, Yang SK, Hnilo JJ, Fiorino M, Potter GL (2002) NCEP–DOE AMIP-II reanalysis (R-2). *Bull Am Meteorol Soc* 83:1631–1643
- Kerns BW, Chen SS (2014) Equatorial dry air intrusion and related synoptic variability in mjo initiation during dynamo. *Mon Weather Rev* 142(3):1326–1343
- Kiladis GN, Dias J, Straub KH, Wheeler MC, Tulich SN, Kikuchi K, Weickmann KM, Ventrice MJ (2014) A comparison of olr and circulation-based indices for tracking the mjo. *Mon Weather Rev* 142(5):1697–1715
- Knutson TR, Weickmann KM (1987) 30–60 days atmospheric oscillations: composite life cycles of convection and circulation anomalies. *Mon Weather Rev* 115(7):1407–1436
- Landu K, Maloney ED (2011) Effect of SST distribution and radiative feedbacks on the simulation of intraseasonal variability in an aquaplanet GCM. *J Meteor Soc Japan* 89(3):195–210. doi:10.2151/jmsj.2011-302
- Lau WKM, Waliser DE (2012) Intraseasonal variability in the atmosphere–ocean climate system. *Environmental Sciences*, edn 2. Springer, Berlin, Heidelberg. doi:10.1007/978-3-642-13914-7
- L’Heureux ML, Higgins RW (2008) Boreal winter links between the Madden–Julian oscillation and the Arctic oscillation. *J Clim* 21(12):3040–3050
- Liebmann B, Hartmann DL (1984) An observational study of tropical–midlatitude interaction on intraseasonal time scales during winter. *J Atmos Sci* 41:3333–3350
- Lin H, Derome J, Brunet G (2007) The nonlinear transient atmospheric response to tropical forcing. *J Clim* 20(22):5642–5665
- Madden RA, Julian PR (1971) Detection of a 40–50 days oscillation in the zonal wind in the tropical Pacific. *J Atmos Sci* 28(5):702–708
- Madden RA, Julian PR (1972) Description of global-scale circulation cells in the tropics with a 40–50 days period. *J Atmos Sci* 29(6):1109–1123
- Maloney ED, Sobel AH (2004) Surface fluxes and ocean coupling in the tropical intraseasonal oscillation. *J Clim* 17(22):4368–4386
- Matthews AJ (2008) Primary and successive events in the Madden–Julian oscillation. *Q J Roy Meteorol Soc* 134(631):439–453
- Matthews AJ, Kiladis GN (1999) The tropical extratropical interaction between high-frequency transients and the Madden Julian oscillation. *Mon Weather Rev* 127:661–667
- Mlawer EJ, Taubman SJ, Brown PD, Iacono MJ, Clough SA (1997) Radiative transfer for inhomogeneous atmospheres: Rrtm, a validated correlated-k model for the longwave. *J Geophys Res: Atmos* (1984–2012) 102(D14), 16663–16682
- Moore RW, Martius O, Spengler T (2010) The modulation of the subtropical and extratropical atmosphere in the pacific basin in response to the Madden Julian oscillation. *Mon Weather Rev preprint* (2010), 0000 (February 2010)
- Noh Y, Cheon W, Hong S, Raasch S (2003) Improvement of the k-profile model for the planetary boundary layer based on large Eddy simulation data. *Bound-Layer Meteorol* 107(2):401–427
- Pan LL, Li T (2008) Interactions between the tropical iso and midlatitude low-frequency flow. *Clim Dyn* 31(4):375–388
- Ray P, Li T (2013) Relative roles of circumnavigating waves and extratropics on the mjo and its relationship with the mean state*. *J Atmos Sci* 70(3):876–893
- Ray P, Zhang C (2010) A case study of the mechanics of extratropical influence on the initiation of the Madden–Julian oscillation. *J Atmos Sci* 67(2):515–528
- Ray P, Zhang C, Dudhia J, Chen SS (2009) A numerical case study on the initiation of the Madden–Julian oscillation. *J Atmos Sci* 66:310–+
- Ray P, Zhang C, Moncrieff MW, Dudhia J, Caron JM, Leung LR, Bruyere C (2011) Role of the atmospheric mean state on the initiation of the Madden–Julian oscillation in a tropical channel model. *Clim Dyn* 36(1–2):161–184
- Reynolds R, Rayner N, Smith T, Stokes D, Wang W (2002) An improved in situ and satellite sst analysis for climate. *J Clim* 15:1609–1625
- Roundy PE (2008) Analysis of convectively coupled Kelvin waves in the Indian Ocean mjo. *J Atmos Sci* 65(4):1342–1359
- Roundy PE (2012) Tropical–extratropical interactions. In: *Intraseasonal variability in the atmosphere–ocean climate system*. Springer, pp 497–512
- Salby M, Hendon HH (1994) Intraseasonal behavior of clouds, temperature, and motion in the tropics. *J Atmos Sci* 51:2207–2224
- Straus DM, Lindzen RS (2000) Planetary-scale baroclinic instability and the mjo. *J Atmos Sci* 57(21):3609–3626
- Vitart F, Jung T (2010) Impact of the northern hemisphere extratropics on the skill in predicting the Madden Julian oscillation. *Geophys Res Lett* 37(23):L23805. doi:10.1029/2010GL045465
- Weickmann K, Berry E (2009) The tropical Madden–Julian oscillation and the global wind oscillation. *Mon Weather Rev* 137(5):1601–1614
- Wheeler M, Kiladis GN (1999) Convectively coupled equatorial waves: analysis of clouds and temperature in the wavenumber–frequency domain. *J Atmos Sci* 56:374–399
- Woolnough S, Vitart F, Balmaseda M et al (2007) The role of the ocean in the Madden–Julian oscillation: implications for mjo prediction. *Q J Roy Meteorol Soc* 133(622):117
- Yanai M, Lu MM (1983) Equatorially trapped waves at the 200 mb level and their association with meridional convergence of wave energy flux. *J Atmos Sci* 40(12):2785–2803
- Yoneyama K, Zhang C, Long CN (2013) Tracking pulses of the Madden–Julian oscillation. *Bull Am Meteorol Soc* 94(12):1871–1891
- Zeng X, Beljaars A (2005) A prognostic scheme of sea surface skin temperature for modeling and data assimilation. *Geophys Res Lett* 32(14):L14605. doi:10.1029/2005GL023030
- Zhang C (2005) Madden–Julian oscillation. *Rev Geophys* 43(2):RG2003. doi:10.1029/2004RG000158
- Zhao C, Li T, Zhou T (2013) Precursor signals and processes associated with mjo initiation over the tropical Indian Ocean*. *J Clim* 26(1):291–307
- Zhou S, Miller AJ (2005) The interaction of the Madden–Julian oscillation and the Arctic oscillation. *J Clim* 18(1):143–159